ORDER, DISORDER, AND PHASE TRANSITIONS IN CONDENSED SYSTEMS

High-Pressure Magnetic Properties and *P–T* Phase Diagram of Iron Borate[¶]

A. G. Gavriliuk[a,b], I. A. Trojan[a], I. S. Lyubutin[b], S. G. Ovchinnikov[c], and V. A. Sarkissian[b]

[a]*Institute for High-Pressure Physics, Troitsk, Moscow oblast, 142190 Russia*
[b]*Institute of Crystallography, Russian Academy of Sciences, Moscow, 119333 Russia*
[c]*Kirensky Institute of Physics, Siberian Division, Russian Academy of Sciences, Krasnoyarsk, 660036 Russia*
e-mail: lyubutin@ns.crys.ras.ru
Received July 6, 2004

Abstract—The high-pressure magnetic states of iron borate $^{57}FeBO_3$ single-crystal and powder samples have been investigated in diamond anvil cells by nuclear forward scattering (NFS) of synchrotron radiation at different temperatures. In the low-pressure ($0 < P < 46$ GPa) antiferromagnetic phase, an increase of the Neél temperature from 350 to 595 K induced by pressure was found. At pressures 46–49 GPa, a transition from the antiferromagnetic to a new magnetic state with a weak magnetic moment (magnetic collapse) was discovered. It is attributed to the electronic transition in Fe^{3+} ions from the high-spin $3d^5$ ($S = 5/2$, $^6A_{1g}$) to the low-spin ($S = 1/2$, $^2T_{2g}$) state (spin crossover) due to the insulator–semiconductor-type transition with extensive suppression of strong d–d electron correlations. At low temperatures, NFS spectra of the high-pressure phase indicate magnetic correlations in the low-spin system with a magnetic ordering temperature of about 50 K. A tentative magnetic P–T phase diagram of $FeBO_3$ is proposed. An important feature of this diagram is the presence of two triple points where magnetic and paramagnetic phases of the high-spin and low-spin states coexist. © *2005 Pleiades Publishing, Inc.*

1. INTRODUCTION

Iron borate $FeBO_3$ is a rare magnetic material that is transparent in the visible range and possesses spontaneous magnetization at room temperature. Light modulation by magneto-optical effects is possible in this crystal. The crystal lattice of $FeBO_3$ has rhombohedral symmetry of the calcite type with the space group $R\bar{3}c$ (D_{3d}^6) and with the lattice parameters $a = 4.612$ Å and $c = 14.47$ Å [1, 2]. Iron ions Fe^{3+} are in oxygen octahedra, and the interionic distances are (Fe–O) = 2.028 Å and (Fe–Fe) = 3.601 Å, while the angles of the bonds (O–Fe–O) are 91.82° and 88.18° [2]. Thus, the oxygen surrounding of Fe is almost cubic. At ambient conditions, $FeBO_3$ is an easy-plane antiferromagnet with weak ferromagnetism and with a Neél temperature of about 348 K [3, 4]. Magnetic moments of two iron sublattices and the weak ferromagnetic moment lie in the basal (111) plane [5, 6].

At ambient pressure, iron borate is an insulator with an optical gap value of 2.9 eV [5]. Recently, a drop in the optical absorption edge approximately from 3 to 0.8 eV has been found in optical spectra at pressures near 46 GPa [7]. It was concluded from direct measurements of electroresistivity that a transition of the insulator–semiconductor type occurs at this pressure [7].

In the present paper, iron borate $^{57}FeBO_3$ single crystals and powder samples are studied under high pressures in a diamond-anvil cell by the technique of nuclear forward scattering (NFS) of synchrotron radiation (SR) in the temperature range 3.5–300 K. At pressures of $P = 46$–49 GPa, the sharp transition from the antiferromagnetic to a new magnetic state with a weak magnetic moment was discovered. The pressure dependence of the Neél temperature was calculated from the experimental data, and the magnetic P–T phase diagram was plotted and analyzed theoretically.

2. EXPERIMENTAL

The perfect quality light-green colored single crystals of $FeBO_3$ enriched with the ^{57}Fe isotope up to 96% were grown by the flux method. The crystals were plate-shaped, and the plane of the plate was the basal (111) plane. The thickness of the plates was about 10–40 μm with dimensions of about 8×8 mm^2. The NFS experiments were performed with both single crystals and powder samples obtained by grinding an $^{57}FeBO_3$ single crystal.

The experiments with nuclear forward scattering of SR were performed with the $^{57}FeBO_3$ samples at high pressures of up to 65 GPa created in diamond-anvil cells at temperatures in the range 3.5–300 K. The measurements were performed with ID18 nuclear reso-

---

[¶] This article was submitted by the authors in English.

nance scattering equipment [8] at the European Synchrotron Radiation Facility (ESRF), Grenoble, France.

Two types of samples were used: a single crystal at room temperature and a powdered sample (a crushed single crystal) at low temperature. At room temperature, a $^{57}FeBO_3$ single crystal with dimensions of about $80 \times 40 \times 4~\mu m^3$ was placed into a high-pressure diamond-anvil cell. The diameter of the working surface of diamonds in the cell was about 300 μm, and the diameter of the hole in the rhenium gasket where the sample was placed was about 100 μm. In the low-temperature experiment, the gasket hole was filled with the sample powder to about one-third to ensure that all powder grains were surrounded by pressure liquid. To create quasi-hydrostatic pressure, the working volume of the cell was filled with PES-5 polyethylsilacsanic liquid. A standard technique of the shift of ruby fluorescence was used to measure the pressure value. For that, several crumbled ruby crystals with dimensions of about 5 μm were placed into the cell along with the sample. They were placed at different distances from the center of the working volume in order to evaluate the pressure gradient in the chamber. The accuracy in the pressure measurements was about 3–4 GPa.

In the NFS experiments, the pressure value was varied up to 65 GPa. The basal plane (111) of the $^{57}FeBO_3$ single crystal was oriented perpendicular to the synchrotron radiation beam, and the vector of polarization of gamma rays was in the sample plane. At every pressure value, the NFS spectra of the powdered sample were measured in the temperature range from 3.5 to 300 K. The Mössbauer time spectra of resonance forward scattering from ^{57}Fe nuclei were measured without an external magnetic field at the sample. The measurements were made in the 16-branch regime.

3. RESULTS AND DISCUSSION

3.1. The Room-Temperature NFS Spectra

Time spectra of the NFS from ^{57}Fe nuclei in $^{57}FeBO_3$ have been recorded at different pressures in the temperature range 3.5–300 K. Figure 1 shows the room-temperature spectra. The spectra represent the intensity of scattered radiation depending on the time following the SR impulse. The damped decay of a nuclear excitation is modulated in time by quantum and dynamic beats. The quantum beats appear due to splitting of nuclear levels by a hyperfine interaction as a result of interference between scattered radiation components of sublevels with different frequencies. The period of quantum beats is inversely proportional to the value of hyperfine splitting energy, and in our case, to the magnetic field value at the iron nuclei. The dynamic beats are due to multiple processes of scattering in a "thick" sample (see details in [9]).

At pressures below 46 GPa, the main feature of the spectra is the evident quantum beats (Fig. 1). Because
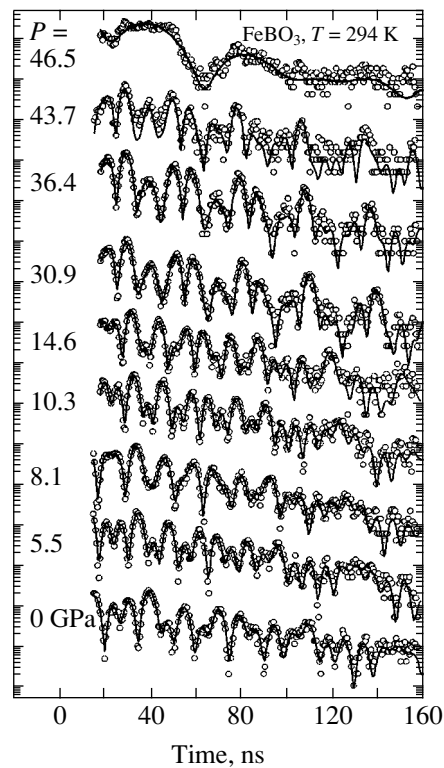

Fig. 1. Room-temperature NFS spectra of the $^{57}FeBO_3$ single crystal at different pressures. Symbols, experimental points; lines, the result of fitting to the MOTIF model.

we used a thin sample, the dynamic beats are not present in the spectra. The NFS spectra were measured with different mutual orientations of the polarization vector of the SR beam and the crystal magnetization. The period of beats is about 8 ns in the case of random orientation of the (111) crystal plane with respect to the direction of the SR-beam polarization and about 15 ns when the crystal is rotated in the basal plane by 90° relative to the first ("random") orientation. The beats with a 15-ns period are 100% modulated, which means that the intensity of scattering in the beats' minimum tends to zero. This indicates that, at all pressures in the range $0 < P < 46$ GPa, the orientation of magnetic fields at the nuclei of iron ions remains in the basal (111) plane of the crystal normal to the radiation beam. At pressures of $P > 46$ GPa, the quantum beats disappear abruptly, showing a drop to zero of the hyperfine magnetic field at ^{57}Fe nuclei.

At ambient pressure, our NFS spectrum is similar to that obtained by Mitsui *et al.* [10] in iron borate. Some distinctions are due to a different thickness of the samples and the absence of an external magnetic field in our measurements.

At $P < 44$ GPa (in the low-pressure (LP) phase of $FeBO_3$), the spectra were processed by the MOTIF program developed by Shvyd'ko [11]. A large number of quantum beats in each spectrum (more than 15) pro-
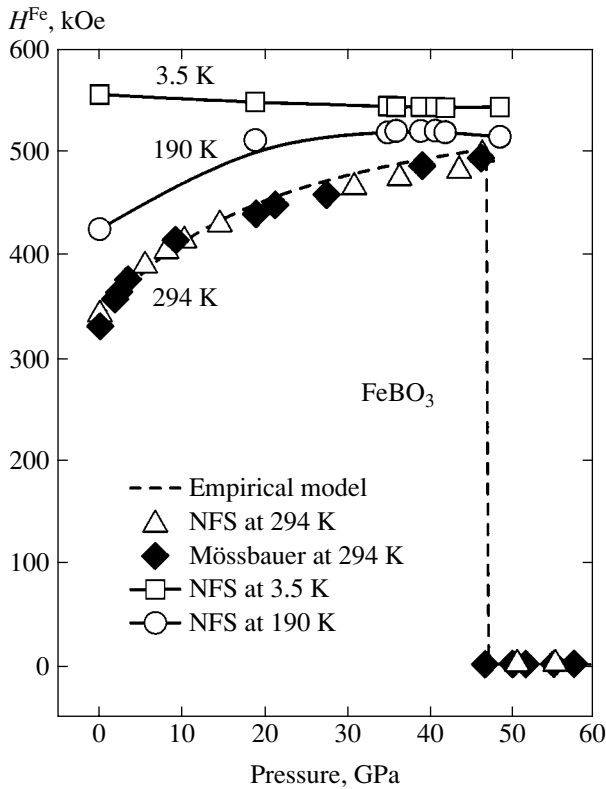
Fig. 2. Pressure dependences of the hyperfine magnetic field H_{hf} at ^{57}Fe nuclei in $FeBO_3$ at different temperatures.

vides high accuracy in determination of the hyperfine magnetic field H_{hf} at iron nuclei (with an error in the range 0.1 T). The H_{hf} values measured at the "random" orientation of the single crystal and after its 90° rotation are the same.

3.2. Magnetic Collapse

The pressure dependences of the hyperfine magnetic field H_{hf} at the iron nuclei are shown in Fig. 2 for different temperatures. At room temperature, the field H_{hf} increases nonlinearly from 34.1 T to its maximum value of 48.1 T as the pressure rises in the range $0 < P < 44$ GPa. At $P = 46–47$ GPa, the field H_{hf} drastically falls down to zero, indicating a magnetic-to-nonmagnetic phase transition (magnetic collapse), obviously of the first-order type. At the transition, the parameter of the quadrupole interaction, which is near zero at $P < 44$ GPa, increases significantly up to 2.1 mm/s.

From the Mössbauer absorption spectra of $^{57}FeBO_3$, we have found that the isomer shift *IS* and quadrupole splitting *QS* of the spectra drastically change at the critical pressure P_c along with the disappearance of the magnetic field H_{hf} (see details in [12]). At $P < 46$ GPa in the low-pressure (LP) phase, the parameters H_{hf}, *IS*, and *QS* are typical of the high-spin ($S = 5/2$) state of Fe^{3+} ions. At $P > 48$ GPa in the high-pressure (HP)

phase of $FeBO_3$, the *IS* and *QS* values become typical of the low-spin state of the Fe^{3+} ions ($S = 1/2$). No indication of the appearance of Fe^{2+} ions was found in the Mössbauer absorption spectra [12]. Thus, the origin of the magnetic collapse at $P = P_c$ is the high-spin (HS) to low-spin (LS) transition of Fe^{3+} ions. A similar conclusion was obtained theoretically in the multielectron model [13], where it was shown that an increase of the crystal field with pressure results in the high-spin–low-spin crossover and an insulator–semiconductor transition.

The NFS spectra at temperatures 77 and 3.5 K are shown in Fig. 3 for different pressures. At $P > 48$ GPa, the effect of the disappearance of quantum beats is clearly seen in the low-temperature spectra. This indicates that the pressure-induced magnetic collapse is not an effect of the temperature but is due to changes in the electronic structure of iron ions. We also observed that, after this transition, the light-green color of the $^{57}FeBO_3$ crystal, typical of ambient pressure, disappeared and the crystal became opaque, which suggests an abrupt drop in the optical absorption gap. The drop of the optical absorption edge has been found recently in optical spectra at pressures just near 46 GPa [7].

At $P < 46$ GPa, the quantum beats in the NFS spectra of the powder sample cannot be fit perfectly to the calculated curves (Fig. 3) as for the single-crystal sample (Fig. 1). This is because the MOTIF program is not developed enough for powder samples when a distribution of magnetic moment and crystal field directions occurs in powder particles. Nevertheless, the frequencies of beats and, hence, the values of the hyperfine magnetic field H_{hf} at iron nuclei can be obtained with a rather high accuracy (with an error in the range of 0.4 T, which is within the limit of a symbol size in Fig. 2).

The pressure dependences of the field H_{hf} at low temperatures are shown in Fig. 2. Contrary to the room-temperature behavior, the field H_{hf} at $T = 3.5$ K in the LP phase is almost constant at a saturation value of about 55.5 T. In fact, the value of H_{hf} even decreases slightly as the pressure increases. This effect can be easily explained by an increase of the covalence contribution to H_{hf} due to decreasing interionic Fe–O distances. It was found that the critical pressure value P_c at which the magnetic transition occurs varies slightly with temperature and P_c becomes somewhat larger at helium temperature.

3.3. Pressure Dependence of the Neél Temperature in the Low-Pressure Phase

In the low-pressure phase of $FeBO_3$, the room-temperature NFS spectra show an increase of the field H_{hf} as the pressure increases. The magnetic field increase is naturally connected with an increase of the exchange interaction, which, in turn, must correlate with the increase in the Neél temperature T_N. In general, the
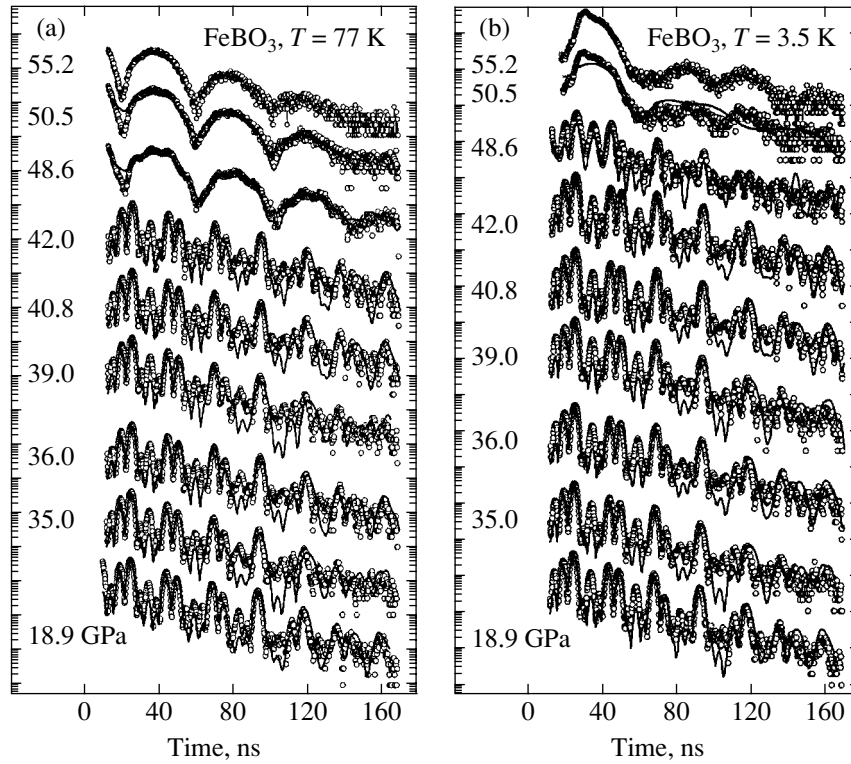
Fig. 3. NFS spectra of the ^{57}FeBO$_3$ powder sample at different pressures: (a) $T = 77$ K, (b) $T = 3.5$ K. Symbols, experimental points; lines, the result of fitting to the MOTIF model.
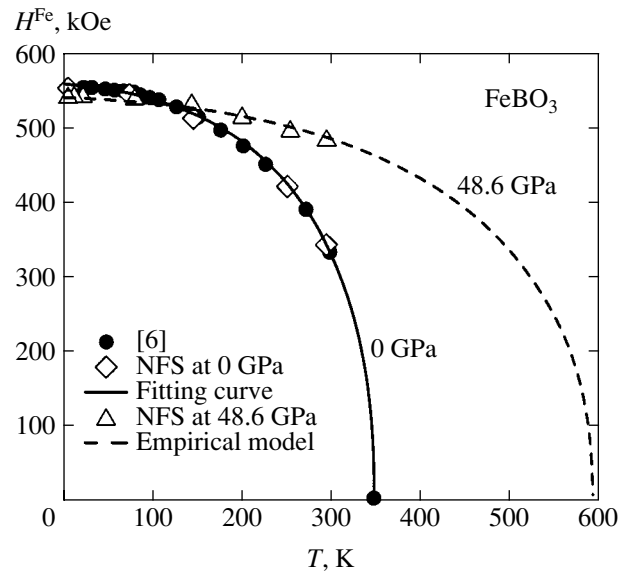
pressure dependence of H_{hf} at room temperature is under the influence of two effects: the changes in T_N and a possible change of the saturation value of H_{hf} at 0 K [$H_{hf}(0)$]. The NFS spectra in the LP phase indicate that, at 3.5 K, the $H_{hf}(0)$ value only slightly depends on pressure. Then, starting with the room-temperature $H_{hf} = f(P)$ dependence and using the ambient-pressure $H_{hf} = F(T)$ dependence (which has been studied in detail by Eibschuts and Lines [6]), we can calculate the dependence of T_N on pressure. For that, we used an extrapolation procedure first suggested in [14, 15] and successfully applied to many experimental results.

We take $H_{hf}(P, T)$ as the empirical function

$$H_{hf}(P, T) = H_{hf}(P, 0)$$
$$\times \exp\left(-\alpha\frac{T}{T_N(P)}\right)\left[1 - \frac{T}{T_N(P)}\right]^\beta. \quad (1)$$

The parameters α and β can be found from the fit of (1) to the experimental dependence $H_{hf}(T)$ at ambient pressure. Using the $H_{hf}(T)$ values for FeBO$_3$ in [6], we found $\alpha = -0.371$ and $\beta = 0.4308$. Then, we assume that α and β are independent of the pressure and take the experimental value $H_{hf}(P, 0) = 55.5$ T. For each experimental value of pressure and the corresponding values

of $H_{hf}(P, T)$, Eq. (1) can be solved graphically for T_N. Figure 4 illustrates the calculation procedure, and the obtained pressure dependence of T_N is shown in Fig. 5.

Fig. 4. Procedure for calculating the Neél temperature of FeBO$_3$ at different pressures by fitting the empirical function to the experimental temperature dependence of the hyperfine magnetic field at ^{57}Fe nuclei.

T_N, K

FeBO$_3$

△ Extrapolation from NFS
◆ Raman [17]
● Magnetization [16]
— Linear fit
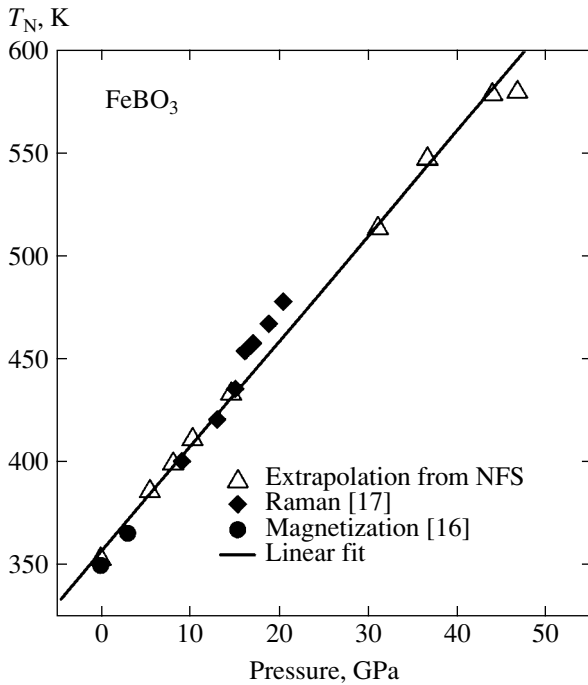
Pressure, GPa

Fig. 5. Pressure dependence of the Neél temperature of FeBO$_3$ from NFS, Raman scattering, and magnetization experiments (symbols). The solid curve corresponds to the pressure slope $dT_N/dP = 5.14$ K/GPa.

In the pressure range $0 < P < 46$ GPa, the dependence $T_N(P)$ can be well fit to a linear function $T_N(P) = T_N(0) + P(dT_N/dP)$, with the parameters $T_N(0) = 355.0 \pm 1.5$ K and $dT_N/dP = 5.14 \pm 0.10$ K/GPa. The arrow value follows from the least-square fit. The maximum value of T_N, attained just before the magnetic collapse, is about 595 K.

From the magnetization measurements of FeBO$_3$ in the range of 0–3 kbar, Wilson and Broersma [16] have found that T_N grows linearly with the slope $dT_N/dP = 5.3$ K/GPa, which is close to our value. Massey *et al.* [17] measured the shift of the two-magnon Raman frequency Ω with the pressure increase in FeBO$_3$ at 99 K. In the range 0–13 GPa, the frequency shift can be approximated by a linear law $\Omega(P) = \Omega(0) + d\Omega/dP$, where $\Omega(0) = 530 \pm 20$ cm^{-1} and $d\Omega/dP = 8.15 \pm 0.7$ cm^{-1}/GPa.

It is interesting to compare the pressure behavior of Ω and T_N. We found that, below 13 GPa, the relative slopes of Ω and T_N are very close: $[1/\Omega(0)]d\Omega/dP = 0.0148$ GPa^{-1} and $[1/T_N(0)]dT_N/dP = 0.0150$ GPa^{-1}. This means that both these parameters are most probably proportional to the superexchange integral J. The $T_N(P)$ data obtained from the magnetization and Raman measurements are also shown in Fig. 5, and they are in good agreement with our studies.

3.4. Magnetic Properties of the High-Pressure Phase

After the magnetic transition, at pressures $P > P_c$, the low-spin state of Fe^{3+} ($S = 1/2$) is not diamagnetic, and one can expect some kind of magnetic correlations at low temperatures. For the HP phase of FeBO$_3$, the recent theoretical calculations of Parlinski [18] predicted a small magnetic moment at iron ions, which is about four times lower than that in the LP phase.

Figure 6 shows our NFS spectra of the powder sample of ^{57}FeBO$_3$ taken at different temperatures with fixed pressures in the HP state (at $P > P_c$). The spectra in Fig. 6c above 50 K are typical of a pure quadrupole interaction without any trace of magnetic modulations. However, at low temperatures, an anomaly appears in the spectra, which cannot be fit to the quadrupole interaction. We tried to fit the NFS spectra at $T < 50$ K with different approximations and have found that the most appropriate is the model of magnetic correlations of Fe^{3+} ions with spin $S = 1/2$, and the magnetic state can be represented as a nonhomogeneous magnetic ordering with a distribution of the H_{hf} field values.

The theoretical calculations in [18] predicted a homogeneous antiferromagnetic ordering at low temperatures for the low-spin HP phase of FeBO$_3$. A nonhomogeneous magnetic state (the low-spin magnetic ordering, LS-MO) found in our experiment may be related to a powder state of the sample due to specific magnetic properties of small particles of FeBO$_3$ at high pressures.

To find the precise temperature of the magnetic ordering in the HP phase, the following procedure was suggested. We fit all spectra in Fig. 6 to the model of pure quadrupole interaction and plot the obtained quadrupole splitting parameter QS as a function of temperature (see Fig. 7). In the pure paramagnetic state, at $T > 50$ K, the QS value is constant. When magnetic correlation appears, the "QS value" found this way starts to increase (Fig. 7), showing a deviation from the model. The point of deviation of QS from the constant value is then taken as the magnetic ordering temperature T_m of the low-spin HP phase.

3.5. Magnetic P–T Phase Diagram of FeBO$_3$

On the basis of all the data obtained, we can plot a tentative magnetic P–T phase diagram (Fig. 8), which shows various magnetic states of FeBO$_3$ at different pressures and temperatures. The almost vertical line at $P = P_c$ separates the left-hand HS insulating low-pressure phase and the right-hand LS semiconducting high-pressure phase. At $P < 46$ GPa, in the high-spin low-pressure phase, the T_N line separates the $T < T_N$ antiferromagnetic (AF) state and the $T > T_N$ paramagnetic (PM) state. At $P > 49$ GPa, in the high-pressure phase,
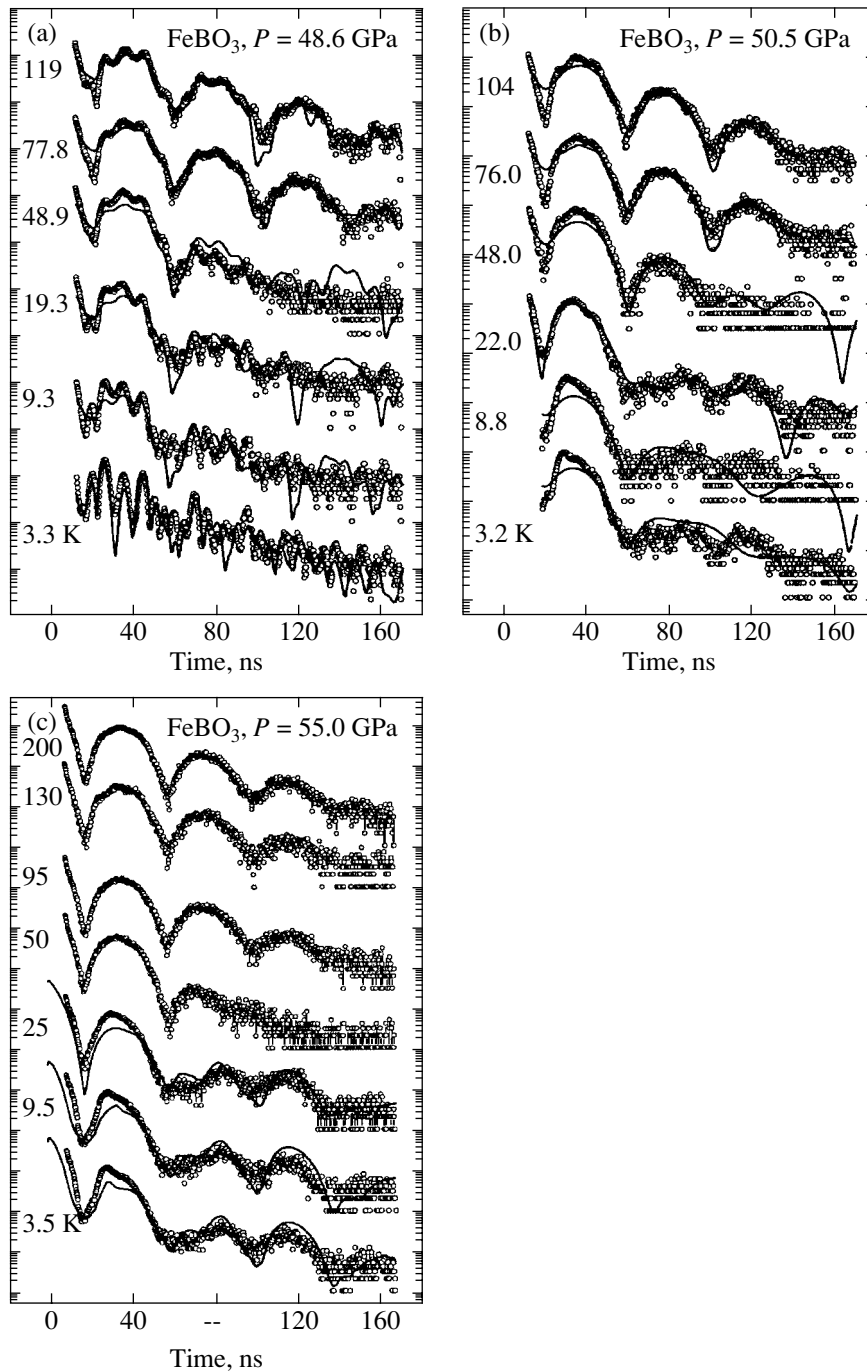
Fig. 6. NFS spectra of a powder $^{57}FeBO_3$ sample for different temperatures with the pressure values fixed at 48.6, 50.5, and 55 GPa. In the HP phase at 55 GPa, the spectra at 3.5, 9.5, and 25 K were fitted to the model of nonhomogeneous magnetic ordering of Fe^{3+} ions with spin $S = 1/2$, and with a distribution of the H_{hf} field values.

the T_m line separates the $T < T_m$ low-spin magnetically ordered state and the $T > T_m$ paramagnetic low-spin state.

An important conclusion follows from the diagram: one can expect two triple points with the coordinates ($P = 46$ GPa, $T = 600$ K) and ($P = 49$ GPa, $T = 50$ K),

where three phases coexist. At the first point, the high-spin antiferromagnetic (HS-AF) and high-spin paramagnetic (HS-PM) phases coexist with the low-spin paramagnetic (LS-PM) phase. At the second point, the low-spin magnetically-ordered (LS-MO) and low-spin paramagnetic (LS-PM) phases coexist with the high-spin antiferromagnetic (HS-AF) phase.

4. THEORETICAL APPROACH

Because the crystal is a semiconductor in the HP phase of $FeBO_3$, its magnetic properties can be described in an approximation of the Heisenberg model both below and above the critical pressure P_c. In the mean-field approximation,

$$T_N = JzS(S + 1)/3, \qquad (2)$$

where $z = 6$ is the number of nearest-neighbors of Fe^{3+},
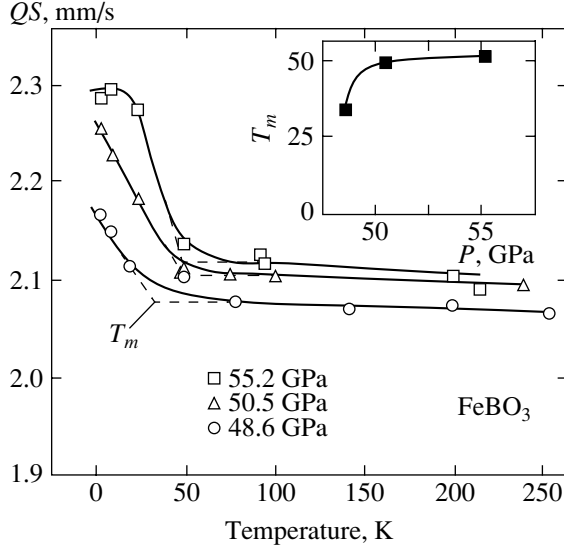
Fig. 7. Temperature dependences of the quadrupole splitting parameter at different pressures in the high-pressure phase of $FeBO_3$ from the fit of the NFS data to the pure quadrupole-interaction model. The point T_m of the deviation from the straight line corresponds to the onset of magnetic ordering of the low-spin HP phase.
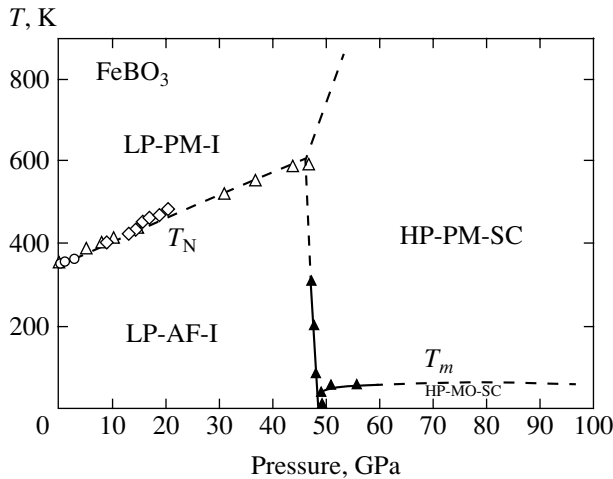
Fig. 8. Tentative magnetic P–T phase diagram of $FeBO_3$. LP-AF-I is the low-pressure antiferromagnetic insulating phase, LP-PM-I is the low-pressure paramagnetic insulating phase, HP-MO-SC is the high-pressure magnetically ordered low-spin semiconducting phase, HP-PM-SC is the high-pressure paramagnetic semiconducting phase. We note the existence of two triple points where three different phases coexist.

the spin $S = 5/2$ characterizes the LP phase, and $S = 1/2$ is the iron spin in the HP phase. The pressure-dependent exchange integral is $J = 2t^2/U_{eff}$, where t is the parameter of the electron jump between nearest Fe^{3+} ions governing the half-width of the d-band, $W_d = zt$, and $U_{eff} = \Omega_c - \Omega_v$ is the effective Hubbard parameter representing the gap between the upper Ω_c (conductivity) and lower Ω_v (valence) Hubbard bands. Here, the upper Hubbard band is the extra electron band due to $d^5 \longrightarrow d^6$ excitations and the lower Hubbard band is the electron removal band due to $d^5 \longrightarrow d^4$ excitations [19]. In the LP phase, both t and U_{eff} parameters depend on pressure as

$$\begin{aligned} t(P) &= t_0 + \alpha_t P, \\ U_{eff}(P) &= U_0 - \alpha_\Delta P, \end{aligned} \qquad (3)$$

where $t_0 = 0.076$ eV and $U_0 = 4.2$ eV are the ambient pressure parameters [19]. The value of the pressure derivative of the crystal field Δ, $\alpha_\Delta = d\Delta/dP = 0.018$ eV/GPa, is found from the condition of crossover of the high-spin $^6A_1$ and low-spin $^2T_2$ terms at $P = P_c$, and the $\alpha_t = dt/dP = 0.00046$ eV/GPa value is found from the rise of T_N from 350 up to 600 K in the LP phase. These values of the derivatives ensure the increase of T_N in the LP phase and the collapse of the Fe^{3+} magnetic moment at P_c.

We now consider the change in magnetic properties of $FeBO_3$ under transition into the HP phase. Near P_c, a structural transition occurs with a jump of unit-cell parameters [20], and, therefore, a jump in the t and U_{eff} values can be expected.

We use "+" to denote the values of parameters on the right-hand side of P_c and "–" to denote those on the left-hand side. Then,

$$\begin{aligned} t_c^{(+)} &= t_0 + \alpha_t P_c + \delta t, \\ U_{eff}^{(+)} &= U_0 - \alpha_\Delta P_c - \delta U. \end{aligned} \qquad (4)$$

Because the a- and c-unit-cell parameters decrease at the transition [20], the δt and δU values must be positive. Assuming $\delta t/t_0 \ll 1$ and $\delta U/U_0 \ll 1$, we write the exchange integral just after the transition as

$$J_c^{(+)} = J_0 \left[1 + \left(\frac{2\alpha_t}{t_0} + \frac{\alpha_\Delta}{U_0} \right) P_c + 2\frac{\delta t}{t_0} + \frac{\delta U}{U_0} \right], \qquad (5)$$

where

$$J_0 = \frac{2t_0^2}{U_0}.$$

The ratio of T_N above and below the transition is then given by

$$\frac{T_N^{(+)}}{T_N^{(-)}} = \frac{J^{(+)} \cdot 1/2 \cdot 3/2}{J^{(-)} \cdot 5/2 \cdot 7/2} = \frac{3}{35}\left(1 + \frac{2\delta t}{t_0} + \frac{\delta U}{U_0}\right), \quad (6)$$

where

$$T_N^{(-)} = 600 \text{ K}.$$

If the jumps in δt and δU are negligible and the change in T_N is only connected with the spin jump $5/2 \longrightarrow 1/2$, we can evaluate the magnetic ordering temperature of the HP phase as

$$T_N^{(+)} = 3T_N^{(-)}/35 = 51 \text{ K}. \quad (7)$$

Taking δt and δU into account could only increase the $T_N^{(+)}$ value. Thus, (7) is an estimate from below, that is, $T_N^{(+)} \geq 51$ K. It turns out that the experimental value of $T_N^{(+)}$ evaluated in Section 3.4 is about 50 K. This suggests that the δt and δU values are negligibly small.

In the HP phase, U_{eff} depends only on the electron transfer and does not depend on the crystal field and pressure [21], and therefore the pressure dependence of T_N is different from that in the LP phase,

$$T_N(P)/T_N^{(+)} = 1 + 2\alpha_t(P - P_c)/t_0. \quad (8)$$

The slope of $T_N(P)$ in the LP phase

$$\frac{dT_N(P)/T_N(0)}{dP} = \frac{2\alpha_t}{t_0} + \frac{\alpha_\Delta}{U_0} = 0.016 \frac{1}{\text{GPa}} \quad (9)$$

is different from that in the HP phase

$$\frac{dT_N(P)/T_N^{(+)}(P_c)}{dP} = \frac{2\alpha_t}{t_0} = 0.012 \frac{1}{\text{GPa}}. \quad (10)$$

Thus, the slope ratio is 4/3.

Now, the question is: How far is expression (8) valid as the pressure increases further, and what happens above T_N? In the HP phase at $P > P_c$ and $T > T_N$, the $FeBO_3$ crystal is a paramagnetic semiconductor with iron ions Fe^{3+} in the low-spin state ($S = 1/2$). However, with a further pressure increase, the semiconducting gap decreases, and it tends to zero at $P = P_M$, where P_M is the point of the transition into the metallic state. The experimental value of P_M evaluated from the thermoactivation gap is approximately 210 GPa [7].

The same value of P_M was found theoretically [21] in extrapolating the level Ω_c down to the crossing with the top of the valence band ε_v. The corresponding dia-
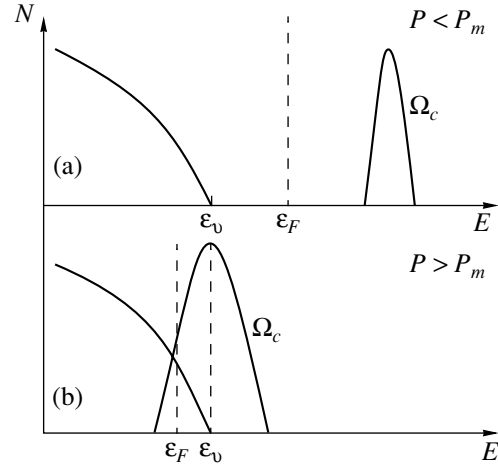
Fig. 9. Diagram of the density of states of $FeBO_3$ at high pressures below (a) and above (b) the semiconductor–metal transition.
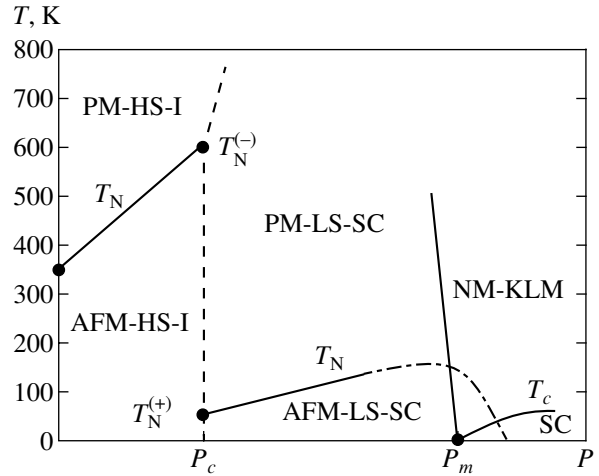
Fig. 10. Supposed phase diagram of $FeBO_3$ at high pressures. AFM, antiferromagnet; PM, paramagnet; HS-I, Fe^{3+} high-spin insulator; LS-SC, low-spin semiconductor; NM-KLM, nonmagnetic Kondo-lattice metal; SC, superconductor.

gram of the electron structure below and above P_M is shown in Fig. 9. Here, the Ω_c level is related to the transitions $[Fe^{(3+)}(d^5), S = 1/2] \longleftrightarrow [Fe^{(2+)}(d6), S = 0]$, and it is smeared into a narrow band due to electron hopping (Fig. 9a). The spin–polaron effect in the antiferromagnetic phase gives rise to a sharp suppression of the d-band width [22].

Above P_M, there are two types of carriers: oxygen holes at the top of the valence band and heavy electrons at the bottom of the d-band. The iron ion is in an intermediate valence state as a mixture of the p^6d^5 and p^5d^6 configurations (Fig. 9b). Because each hole at oxygen gives rise to the $S = 0$ state of the d^6 configuration in iron, one may consider the situation as a peculiar

Kondo effect, when carriers screen the iron spin. Because spins are located regularly, the system can be attributed to a Kondo lattice. At higher temperatures, one can expect a nonmagnetic Kondo metal state; at low temperatures, a competition between antiferromagnetism and superconductivity induced by spin fluctuations can be dominant [23, 24]. The corresponding phase diagram is shown in Fig. 10. Only the magnetic and electron properties of $FeBO_3$ are shown in the diagram, and the structural transitions are not discussed here. We note that, from the standpoint of modern terminology, the P_M point in the diagram of Fig. 10 is a typical quantum critical point.

5. CONCLUSIONS

Both experimentally and theoretically, we have shown that the magnetic collapse in $FeBO_3$ at high pressure does not transform the material into a nonmagnetic state with the disappearance of magnetic properties. At the transition, the low-pressure phase with a strong magnetic interaction transforms into the high-pressure phase with a weak magnetic interaction, and this transformation is accompanied by an insulator–semiconductor transition. The forthcoming metallization and unusual properties of the Kondo lattice metal state are subjects for future experimental study.

ACKNOWLEDGMENTS

REFERENCES

1. Database PDF-II, record 21-0423; I. Bernal, C. W. Struck, and J. G. White, Acta Crystallogr. **16**, 849 (1963).
2. R. Diehl, Solid State Commun. **17**, 743 (1975).
3. R. Wolfe, A. J. Kurtzig, and R. C. LeCraw, J. Appl. Phys. **41**, 1218 (1970).
4. M. Eibschuts, L. Pfeiffer, and J. W. Nielsen, J. Appl. Phys. **41**, 1276 (1970).
5. M. P. Petrov, G. A. Smolenskiǐ, A. P. Pagurt, *et al.*, Fiz. Tverd. Tela (Leningrad) **14**, 109 (1972) [Sov. Phys. Solid State **14**, 87 (1972)].
6. M. Eibschuts and M. E. Lines, Phys. Rev. B **7**, 4907 (1973).
7. I. A. Trojan, M. I. Eremets, A. G. Gavriliuk, *et al.*, JETP Lett. **78**, 13 (2003).
8. R. Ruffer and A. I. Chumakov, Hyperfine Interact. **97/98**, 589 (1996).
9. G. V. Smirnov, Hyperfine Interact. **123/124**, 31 (1999).
10. T. Mitsui, S. Kitao, M. Seto, *et al.*, J. Phys. Soc. Jpn. **68**, 1049 (1999).
11. Yu. V. Shvyd'ko, Phys. Rev. B **59**, 9132 (1999).
12. V. A. Sarkissyan, I. A. Trojan, I. S. Lyubutin, *et al.*, JETP Lett. **76**, 664 (2002).
13. S. G. Ovchinnikov, JETP Lett. **77**, 676 (2003).
14. A. G. Gavriliuk, G. N. Stepanov, V. A. Sidorov, and S. M. Irkaev, J. Appl. Phys. **79**, 2609 (1996).
15. A. G. Gavriliuk, G. N. Stepanov, I. S. Lyubutin, *et al.*, JETP **90**, 330 (2000).
16. D. M. Wilson and S. Broersma, Phys. Rev. B **14**, 1977 (1976).
17. M. J. Massey, R. Merlin, and S. M. Girvin, Phys. Rev. Lett. **69**, 2299 (1992).
18. K. Parlinski, Eur. Phys. J. B **27**, 283 (2002).
19. S. G. Ovchinnikov and V. N. Zabluda, JETP **98**, 135 (2004).
20. A. G. Gavriliuk, I. A. Trojan, R. Boehler, *et al.*, JETP Lett. **75**, 23 (2002).
21. A. G. Gavriliuk, I. A. Trojan, S. G. Ovchinnikov, *et al.*, JETP **99**, 566 (2004).
22. É. A. Nagaev, *Physics of Magnetic Semiconductors* (Nauka, Moscow, 1979) [in Russian].
23. P. Schlottmann, Phys. Rep. **181**, 1 (1989).
24. P. Fulde, *Electron Correlations in Molecules and Solids* (Springer, Berlin, 1991), Springer Ser. Solid-State Sci., Vol. 100.